Supporting Information

Engineering Er^{3+}-sensitized nanocrystal for enhancing the NIR II-responsive upconversion luminescence

Hong Wang[a], Yang Xu[a], Tao Pang[b*], Baojiu Chen[a], Fangyun Xin[a], Mingming Xing[a*], Meng Tian[a], Yao Fu[a], Xixian Luo[a,c], Ying Tian[a*]

[a] School of Science, Dalian Maritime University, Dalian 116026, China

[b] College of Science, Huzhou University, Huzhou 313000, China

[c] Key Laboratory of New Energy and Rare Earth Resource Utilization of State Ethnic Affairs Commission, Key Laboratory of Photosensitive Materials & Devices of Liaoning Province, School of Physics and Materials Engineering, Dalian Minzu University, Dalian 116600, China

E-mail: tpang@126.com (Pang T.), tianying@dlmu.edu.cn (Tian Y.), xingming1112@126.com (Xing M. M.)

Experimental section

Materials

$Y(CH_3COO)_3$ (99.9%), $Er(CH_3COO)_3$ (99.9%), $Yb(CH_3COO)_3$ (99.9%), $Ho(CH_3COO)_3$ (99.9%), $Tm(CH_3COO)_3$ (99.9%), sodium oleate (NaOA; >80%), ammonium fluoride (NH_4F; >98%), 1-octadecene (90%), oleic acid (90%) were all purchased from Sigma-Aldrich. NaOH (99%+) was purchased from Damas-beta. Methanol (A.R.) and cyclohexane (A.R.) were purchased from Sinopharm Chemical Reagent Co., Ltd. All lanthanide raw materials were dissolved in deionized water, while NaOH and NH_4F were dissolved in methanol solution. All the chemicals were used as received without further purification.

Preparation of upconversion nanoparticles

The core-only NPs were prepared via well-established co-precipitation method [1] and modified co-precipitation method [2]. The core-shell NPs were subsequently obtained via epitaxial layer growth technique. The preparation method is detailed as follows:

Synthesis of hexagonal-phase $NaYF_4$:y mol%Yb (y=20, 50, 80, and 100), $NaY_{(1-y)}Yb_yF_4$:Ho (y=18, 48, 78, 98 mol%), $NaYb_{(1-z)}F_4$:zHo (z=2, 4, 6, 8 mol%), and $NaYb_{(1-w)}F_4$:wTm (w=0.5, 1, 2, 3 mol%) nanocrystals

In hexagonal $NaLnF_4$ nanocrystals, the size of nanocrystals would increase with the Yb^{3+} doping concentration due to the rapid growth of hexagonal $NaYbF_4$ crystals [3]. Therefore, a specially modified co-precipitation method was adopted to prepare the $NaYbF_4$ nanocrystals to keep the similar particle sizes [2]. Typically, 0.835 mmol of $Ln(CH_3COO)_3$ (0.2 M), oleic acid (5 mL), and 1-octadecene (5 mL) were added into a two-necked flask (50 mL). The mixture was heated and maintained at 150 ℃ under stirring for 1 h until complete removal of water. Subsequently, NaOA (6.67 mmol) was added to the mixture. The reaction mixture was then heated and kept at 100 ℃ for 1 h under vacuum. Next, the NH_4F (9.185 mmol) was added to the mixture under nitrogen atmosphere. The reaction mixture was reacted at 160 ℃ for 1 h under nitrogen atmosphere and then degassed for 10 min. After that, the reaction was kept at 300 ℃ for 1 h under nitrogen atmosphere and then cooled to room temperature. The as-prepared nanoparticles were collected by centrifugation and washed with ethanol for three times. The solutions obtained were dispersed in cyclohexane and centrifuged to remove the NaF by-product. Finally, the obtained nanoparticles were re-dispersed

in 4 mL of cyclohexane for further use.

Synthesis of hexagonal-phase $NaYF_4$:Yb@$NaYF_4$:x mol%Er@$NaYF_4$ (x= 5, 10, 20, 30, 40) core-shell nanoparticles. NaY(1-y)YbyF$_4$:2%Ho@$NaYF_4$:Er@$NaYF_4$ (y=18, 48, 78, 98 mol%), $NaYb_{(1-z)}F_4$:zHo@$NaYF_4$:Er@$NaYF_4$ (z=2, 4, 6, 8 mol%), and $NaYb_{(1-w)}F_4$:wTm@$NaYF_4$:Er@$NaYF_4$ (w=0.5, 1, 2, 3 mol%) nanocrystals

In a typical procedure of preparing the core-shell nanoparticles, a mixture of 3 mL of oleic acid, 7 mL of 1-octadecylene, and 2 ml of aqueous solution containing a total amount of 0.4 mmol lanthanide with particular ratios were added into a 50-mL two-necked flask. The reaction solution was heated at 150 ℃ for 1 h and then cooled to room temperature. Then the as-prepared $NaYF_4$:Yb core solution was added into the reaction mixture. Subsequently, a methanol solution (6 mL) containing NaOH (1 mmol) and NH_4F (1.6 mmol) was added and stirred at 50 ℃ for 45 min. After the methanol was evaporated at 100 ℃. Afterwards, the reaction solution was then heated to 300 ℃ for 1.5 h under nitrogen atmosphere. The as-prepared nanoparticles were collected by centrifugation, washed with ethanol for three times, and finally re-dispersed in 4 mL of cyclohexane.

The synthesis procedure of the core-shell-shell nanoparticles was similar to that of the above core-shell nanoparticles except different core and lanthanide precusor as core and shell layer, respectively.

Synthesis of hexagonal-phase $NaYF_4$:Er@$NaYF_4$, $NaYF_4$:Er,Yb@$NaYF_4$, $NaYF_4$:Yb,Ho@$NaYF_4$, $NaYF_4$:Er,Ho@$NaYF_4$, $NaYF_4$:Er,Yb,Ho@$NaYF_4$, $NaYF_4$:Er,Tm@$NaYF_4$, and $NaYF_4$:Er,Yb,Tm@$NaYF_4$ core-shell nanoparticles

Typically for the procedure of preparing the core nanoparticles, a mixture of oleic acid (3 ml), 1-octadecylene (7 ml), and 2 ml of aqueous solution containing a total amount of 0.4 mmol lanthanide with particularly designed ratios were added into a two-necked flask (50 ml). The reaction solution was heated to 150 ℃ and maintained for 60 min, during which keep the bottleneck open and magneton stirring to remove residual water and oxygen. Next, the reaction mixture was cooled to room temperature. Then a mixture of 1 ml NaOH (1M) and 4 ml NH_4F (0.4 M) (methanol solution) was poured into the two-necked flask. The mixture solutions was heated to 50 ℃ for 45 min. The resulting transparent solution was continuously heated to 290 ℃ for 1.5 h under nitrogen atmosphere. When cooling to room temperature, the core nanocrystals were washed with absolute ethanol and cyclohexane for at least twice

and dispersed in 4 mL cyclohexane. For the core-shell nanoparticles, 4 mL of core nanoparticles solution was used as shell precursor.

Synthesis of hexagonal-phase $NaYF_4$:Ho@$NaYF_4$:Er,Yb@$NaYF_4$, $NaYF_4$:Ho@$NaYF_4$:Er@$NaYF_4$, $NaYF_4$:Yb,Ho@$NaY_{(1-x)}F_4$:xEr@$NaYF_4$ (x=5, 10, 20, 30, 50, 80, 100 mol%), $NaYF_4$:Yb,Ho@$NaYF_4$:Er,Yb@$NaYF_4$, $NaYF_4$:Tm@$NaYF_4$:Er@$NaYF_4$, $NaYF_4$:Tm@$NaYF_4$:Er,Yb@$NaYF_4$, $NaYF_4$:Yb,Tm@$NaYF_4$:Er@$NaYF_4$, and $NaYF_4$:Yb,Tm@$NaYF_4$:Er,Yb@$NaYF_4$ core-shell-shell nanoparticles

The procedure was similar to the synthesis of core-shell nanoparticles except different nanoparticles as core were used to coated on shell during the experiment.

Synthesis of hexagonal-phase $NaYF_4$:Yb,Tm@$NaYF_4$:Er,Yb@$NaYF_4$:Yb@$NaYF_4$ core-shell-shell-shell nanoparticles

The synthesis procedure was identical to that of the above-mentioned core-shell-shell nanoparticles except for the use of different core nanoparticles and corresponding lanthanide shell precursors.

Characterization

XRD data of the samples were performed using a LabX XRD-6000 X-ray generator with Cu-Ka radiation. TEM images were obtained using a JEM 2100F high-resolution electron microscope. EDS was carried out on an FEI Tecnai G2 F20 S-TWIN transmission electron microscope. Ultraviolet-visible-near infrared (UV-vis-NIR) absorption spectra of the solutions were obtained using Shimadzu UV-2600 UV-vis spectrophotometer. Fluorescence spectra were recorded by Andor fluorescence spectrophotometer (Andor Kymera 193i-B2) equipped with DU420A-OE and DU490A-1.7 detectors, and Edinburgh FS5 fluorescence spectrophotometer equipped with R928P detector. The upconversion luminescent efficiencies of the sample were measured by using the fluorescence spectrophotometer (Andor Kymera 193i-B2) equipped with DU490A-1.7 detector and an integrating sphere setup. The luminescence lifetime decay of Er^{3+} ions was examined with HJY TRIAX550 spectrophotometer. Excitation sources were power-tunable 1550 nm laser diode. The digital photos were recorded by iPhone 11.

Supplementary Text

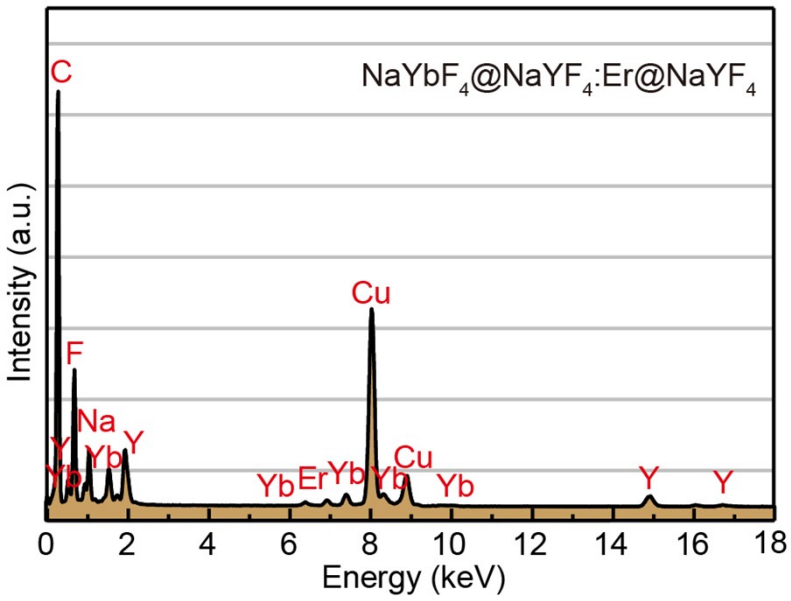

Fig. S1 EDS spectrum of the as-synthesized Yb@Er@Y upconversion nanoparticles. The strong signal of Cu and C elements are from original TEM copper grid and the OA ligand on the particle surface, respectively.

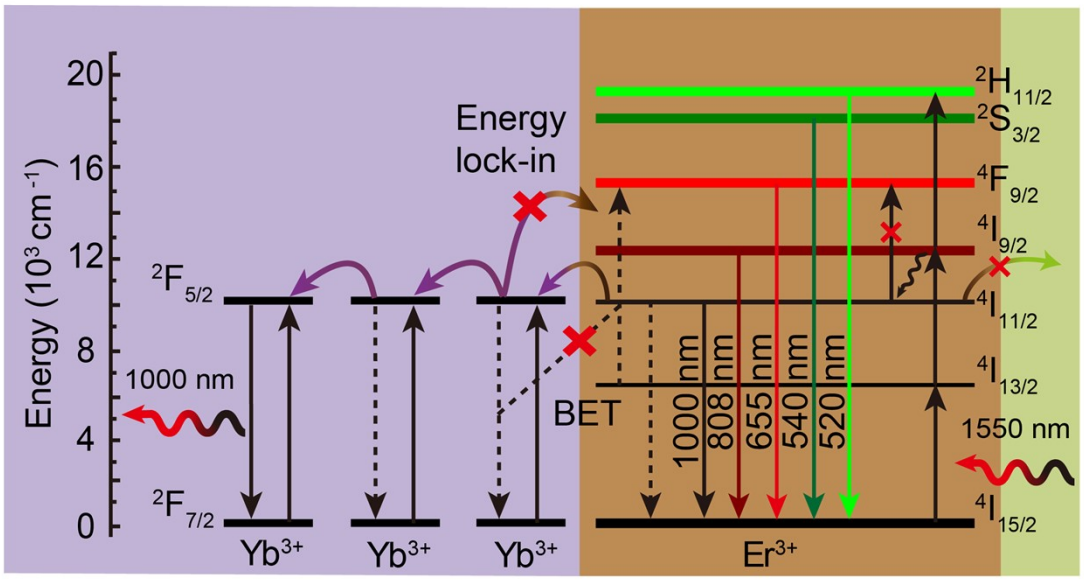

Fig. S2 Upconversion luminescence mechanisms for the Yb@Er@Y sample. The 520, 550, 655, and 808 nm emissions are assigned to the transitions from the $^2H_{11/2}$, $^4S_{3/2}$, $^4F_{9/2}$, and $^4I_{9/2}$ states to the ground $^4I_{15/2}$ state of Er^{3+}, respectively. The 1000 nm emissions come from the transitions from the $^4I_{11/2}$ to $^4I_{15/2}$ state of Er^{3+} and $^2F_{5/2}$ to $^2F_{7/2}$ state of Yb^{3+}.

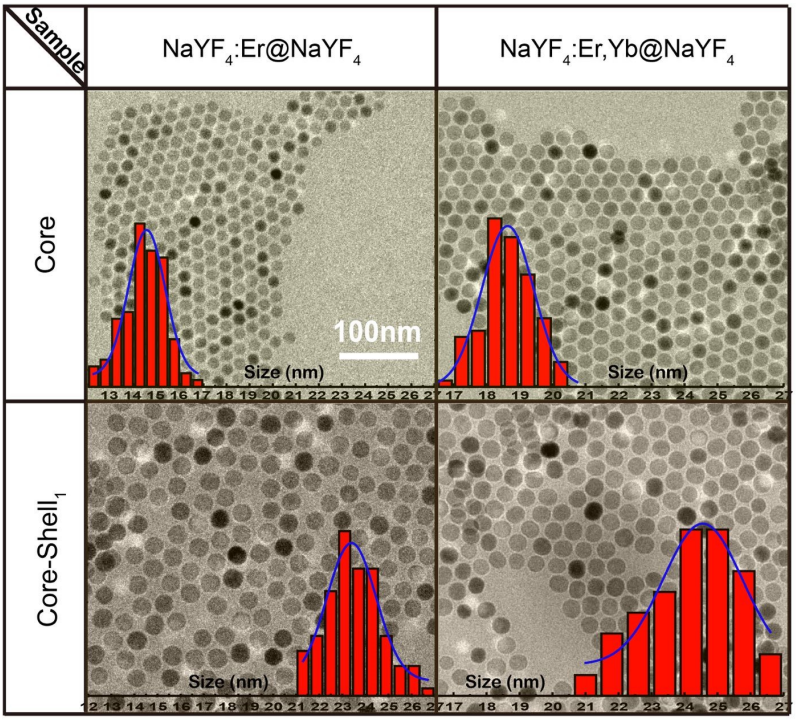

Fig. S3 TEM images and the corresponding size distributions (inset) of Er@Y and Er,Yb@Y upconversion nanoparticles.

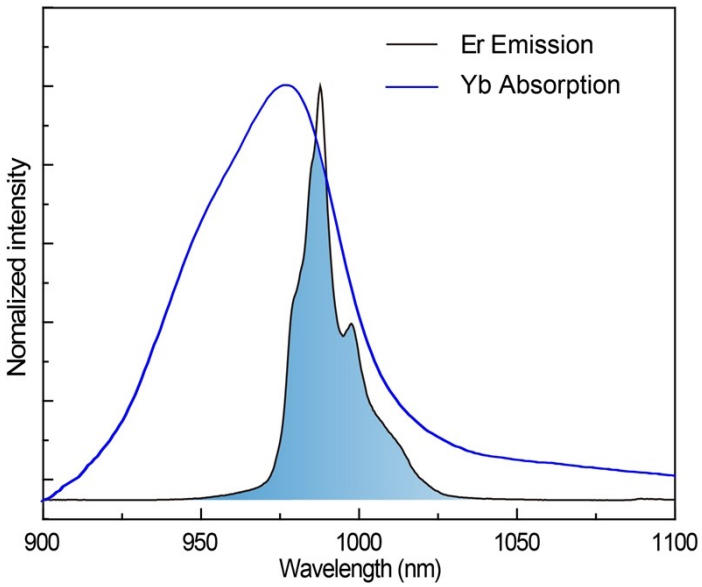

Fig. S4 Normalized NIR absorption spectrum of Yb^{3+} ($^2F_{7/2}\rightarrow{}^2F_{5/2}$ transition) and the emission spectrum of Er^{3+} ($^4I_{11/2}\rightarrow{}^4I_{15/2}$ transition). The large absorption cross section of Yb^{3+} $^2F_{7/2}\rightarrow{}^2F_{5/2}$ transition overlaps well with the emission of Er^{3+} $^4I_{11/2}\rightarrow{}^4I_{15/2}$ transition, thus allowing resonant ET from Er^{3+} $^4I_{11/2}$ to Yb^{3+} $^2F_{5/2}$.

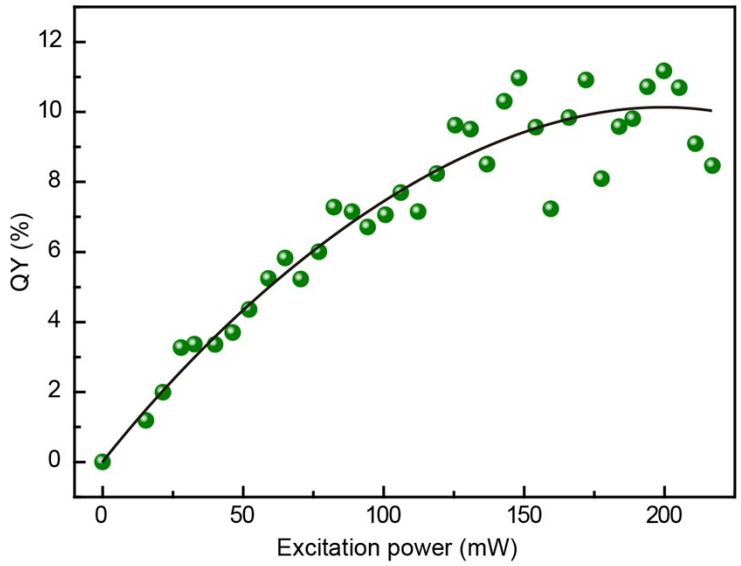

Fig. S5 The dependence of upconversion luminescence QY of the Yb@Er@Y sample as a function of 1550 nm excitation power. The blank chloroform solution was used as the reference sample. The QY of upconversion luminescence was calculated based on the equation of QY= $[E_{sam} - E_{ref}] / [L_{ref} - L_{sam}]$ [4,5], where E_{sam}, E_{ref}, L_{sam}, L_{ref} are sample emission, reference sample emission, sample excitation scattering, and reference sample excitation scattering, respectively. The QY of upconversion luminescence continuously enhances with the excitation power from 15 to 148 mW. When increase the power over 148 mW, the luminescent efficiency cannot further enhance due to the saturation of the excited energy levels of the rare earth ions [6-8].

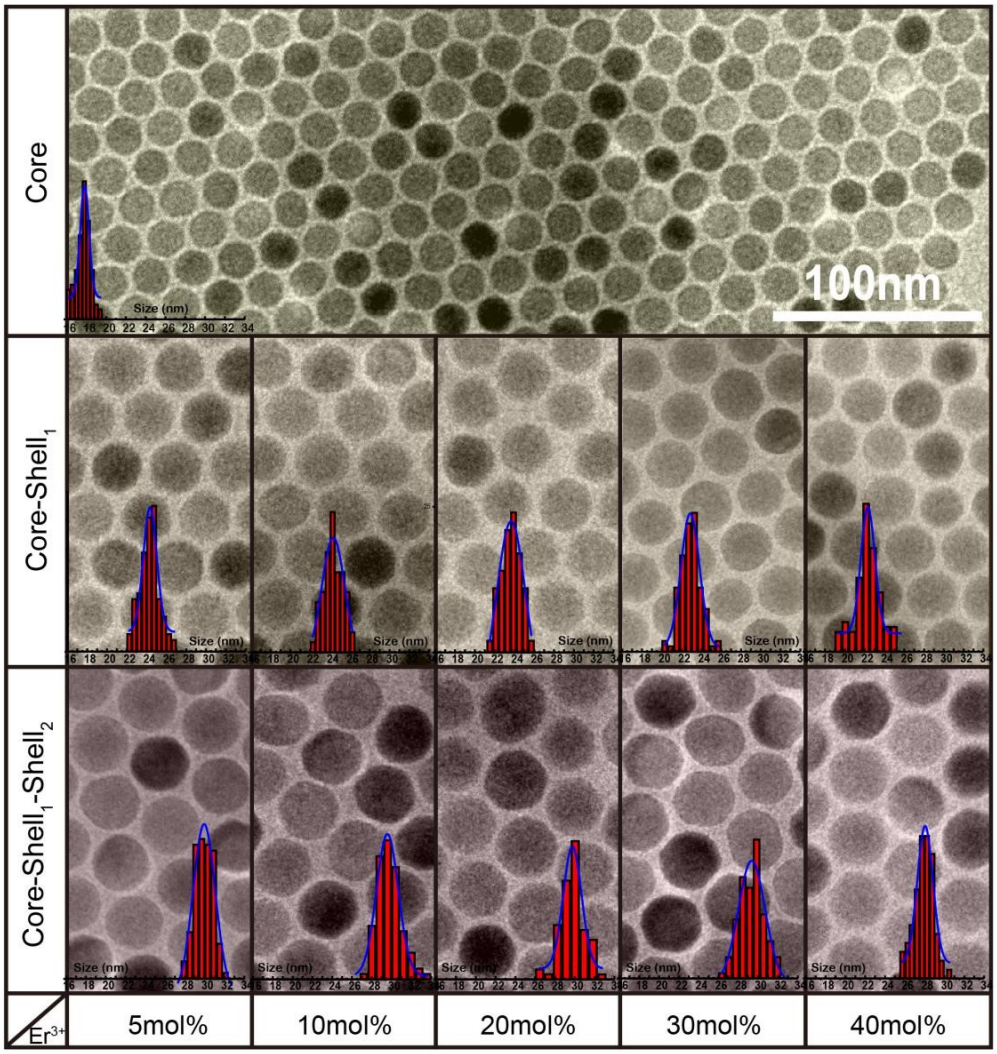

Fig. S6 TEM images and the corresponding size distributions (inset) of Yb^{3+}-doped core, Yb@xEr (x=5, 10, 20, 30, 40 mol%) core-shell, and Yb@xEr@Y core-shell-shell nanoparticles.

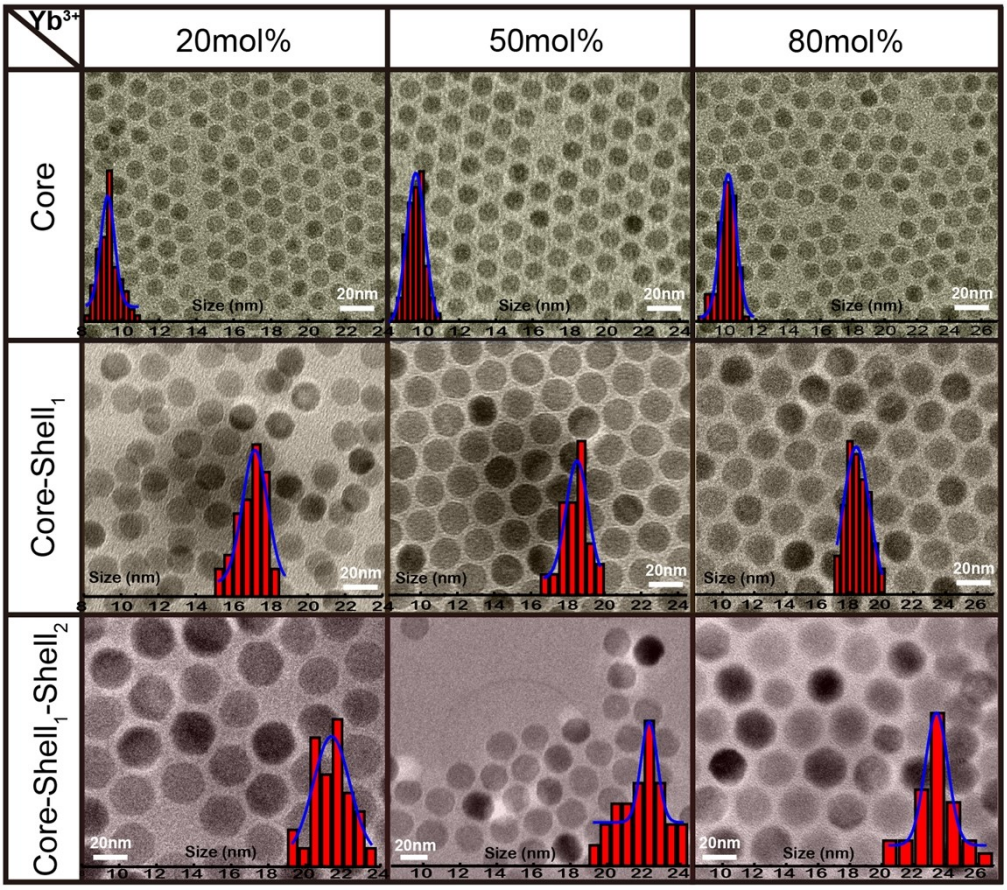

Fig. S7 TEM images and the corresponding size distributions (inset) of yYb^{3+}-doped (y=20, 50, 80, 100 mol%) core, yYb@Er core-shell, and yYb@Er@Y core-shell-shell nanoparticles.

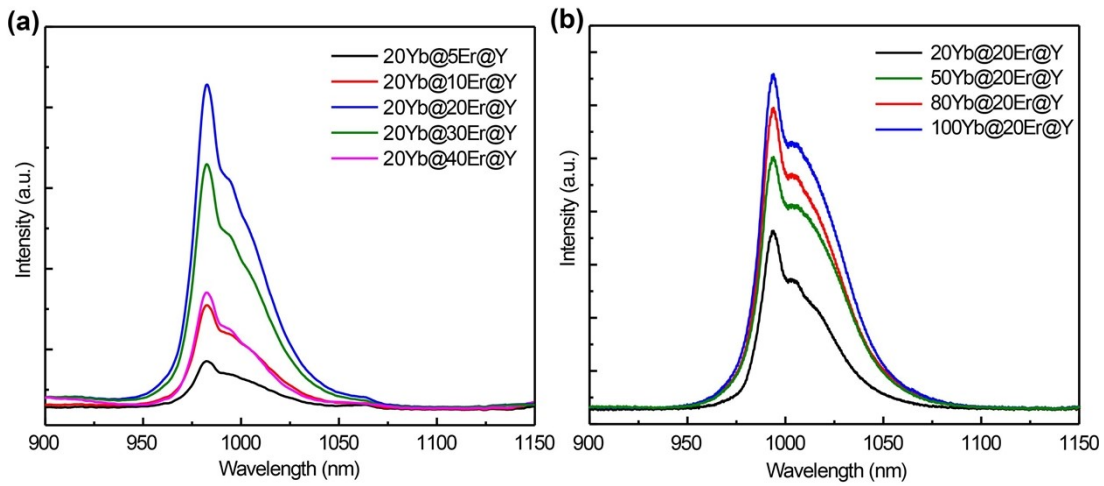

Fig. S8 Upconversion emission spectra of (a) 20%Yb@xEr@Y (x=5, 10, 20, 30, 40 mol%) and (b) yYb@20%Er@Y (y=20, 50, 80, 100 mol%) upconversion nanoparticles under 1550 nm excitation. When varying the Er^{3+} concentrations from 5 to 40% at a fixed Yb^{3+} concentration of 20%, the luminescence intensity of the nanoparticles reaches the maximum at the concentration of 20%Er^{3+}. Using 20%Er^{3+} as the optimum concentration, the Yb^{3+} ion concentration varies from 20 to 100%. The result shows that the 100%Yb@20%Er@Y sample displays the strongest emission intensity, resulting from a larger number of emitters to generate luminescence with increasing of Yb^{3+} doping concentration.

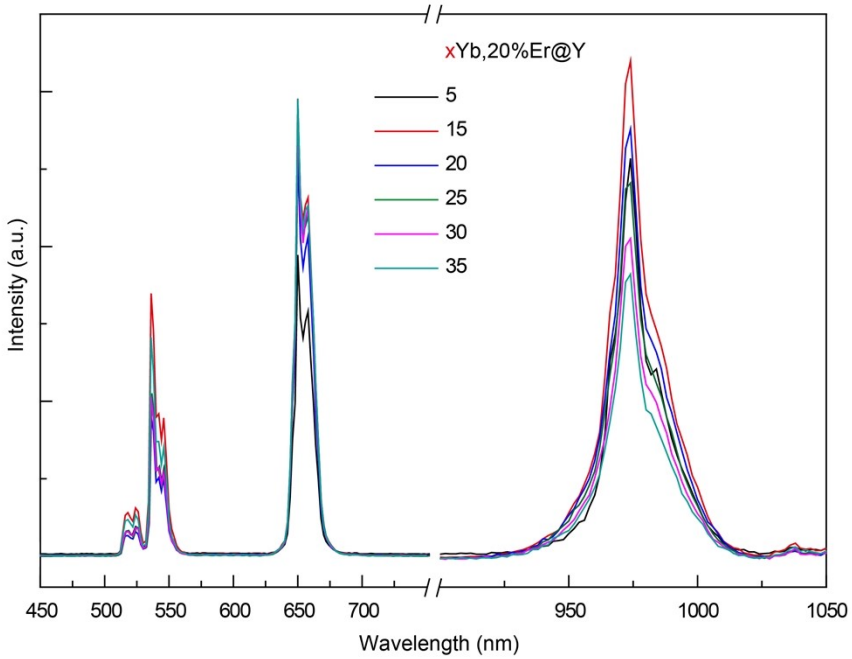

Fig. S9 Upconversion emission spectra of xYb,20%Er@Y (x=5, 15, 20, 25, 30, 35 mol%) nanoparticles under 1550 nm excitation.

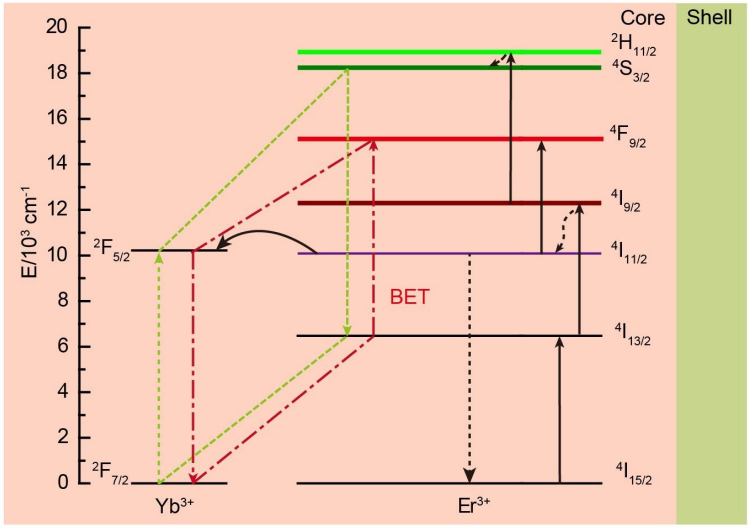

Fig. S10 Schematic upconversion processes in Yb,Er@Y nanoparticles under 1550 nm excitation.

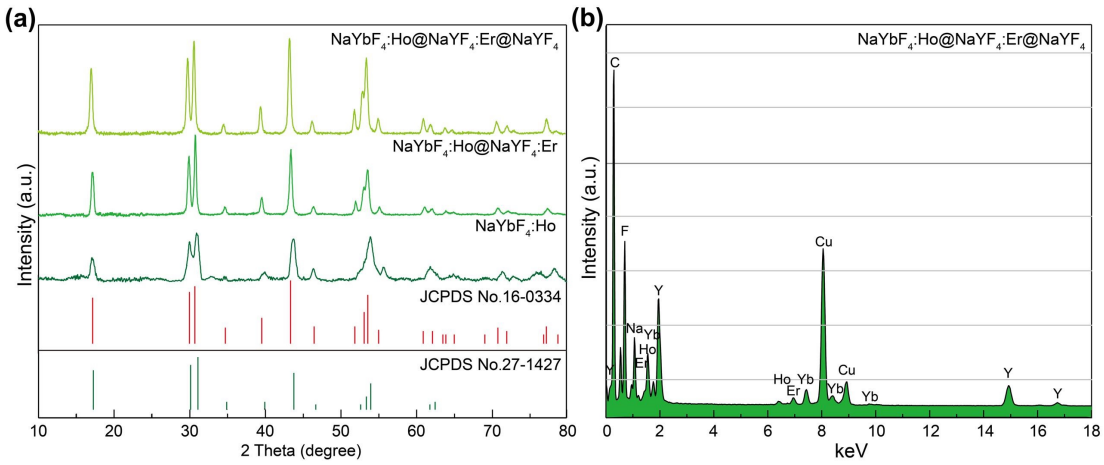

Fig. S11 (a) XRD patterns of Yb,Ho core, Yb,Ho@Er core-shell, and Yb,Ho@Er@Y core-shell-shell nanoparticles. (b) EDS spectrum of Yb,Ho@Er@Y nanoparticles. The XRD results prove the as-synthesized samples to be pure hexagonal phase. All the elements of Na^{+}, F^{-}, Y^{3+}, Ho^{3+}, Yb^{3+}, and Er^{3+} elements were detected by the EDS analysis. The strong signal of Cu and C elements are from original TEM copper grid and the OA ligand on the particle surface, respectively.

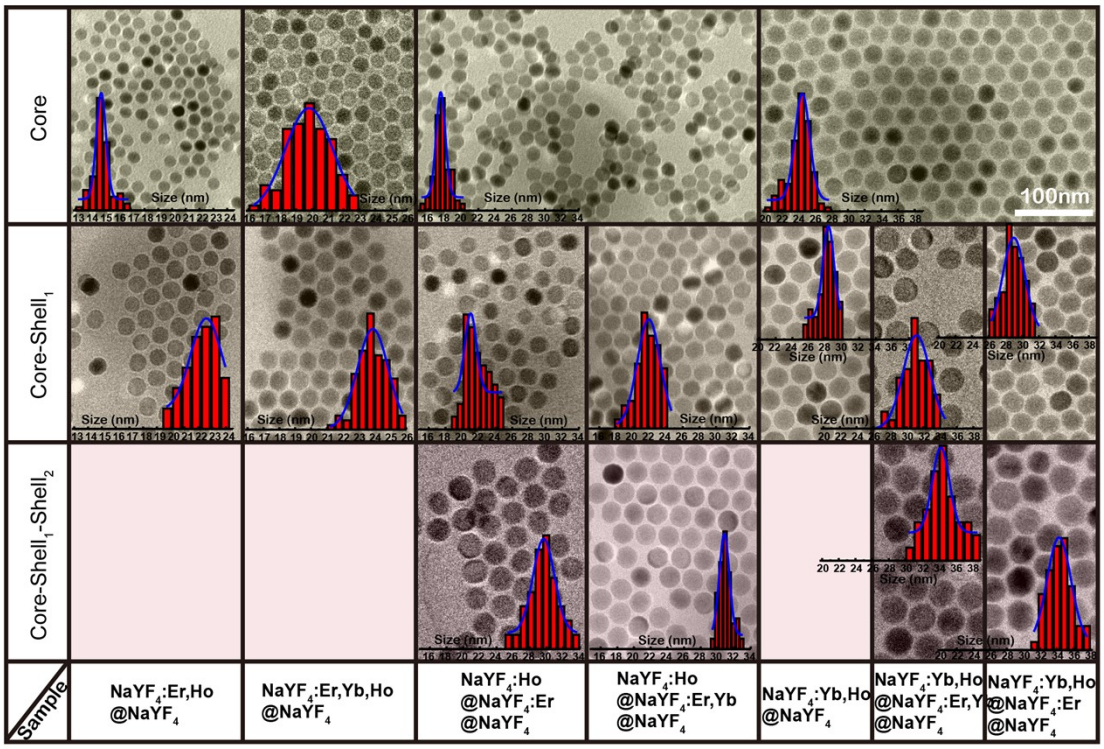

Fig. S12 TEM images and the corresponding size distributions (inset) of Er,Ho@Y, Er,Yb,Ho@Y, Ho@Er@Y, Ho@Er,Yb@Y, Yb,Ho@Y, Yb,Ho@Er,Yb@Y, and Yb,Ho@Er@Y nanoparticles.

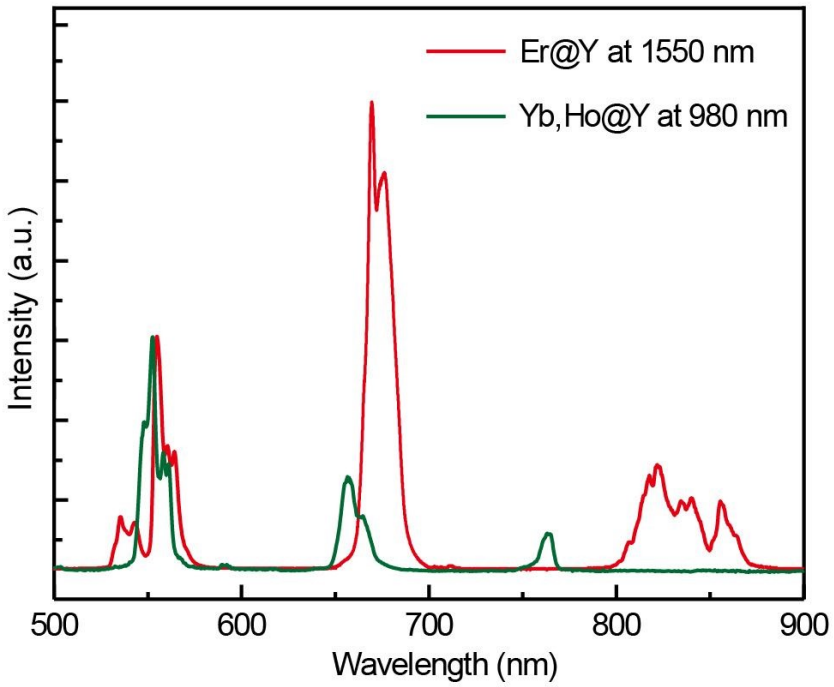

Fig. S13 Upconversion emission spectra of Er@Y excited by 1550 nm laser and Yb,Ho@Y excited by 980 nm laser. The Er^{3+} and Ho^{3+} ions both show the green and red upconversion emissions. While the wavelengths of the two peaks of Ho^{3+} move to the left compared with that of Er^{3+} ions.

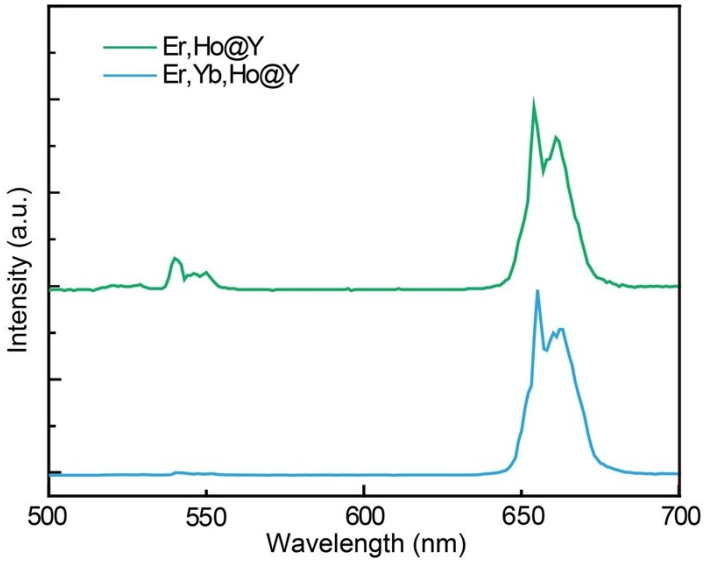

Fig. S14 The upconversion spectra of Er,Ho@Y and Er,Yb,Ho@Y samples in the visible region under 1550 nm excitation.

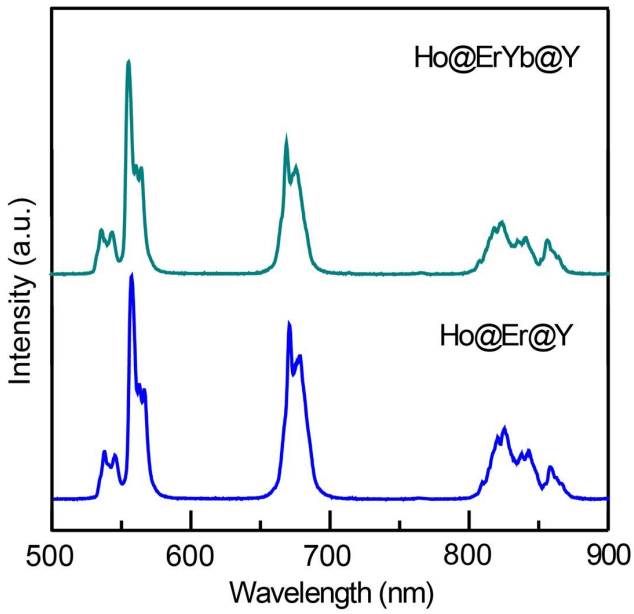

Fig. S15 Upconversion emission spectra of Ho@Er@Y and Ho@Er,Yb@Y nanoparticles under 1550 nm excitation.

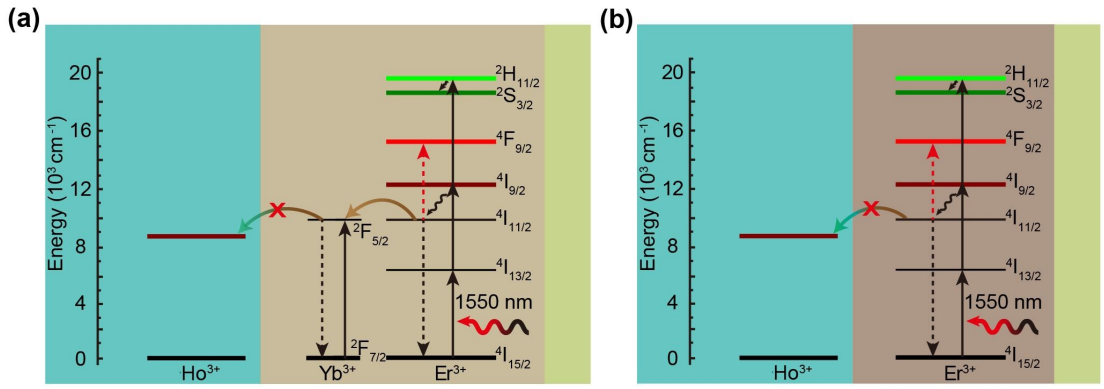

Fig. S16 Schematic upconversion processes in (a) Ho@Er@Y and (b) Ho@Er,Yb@Y nanoparticles.

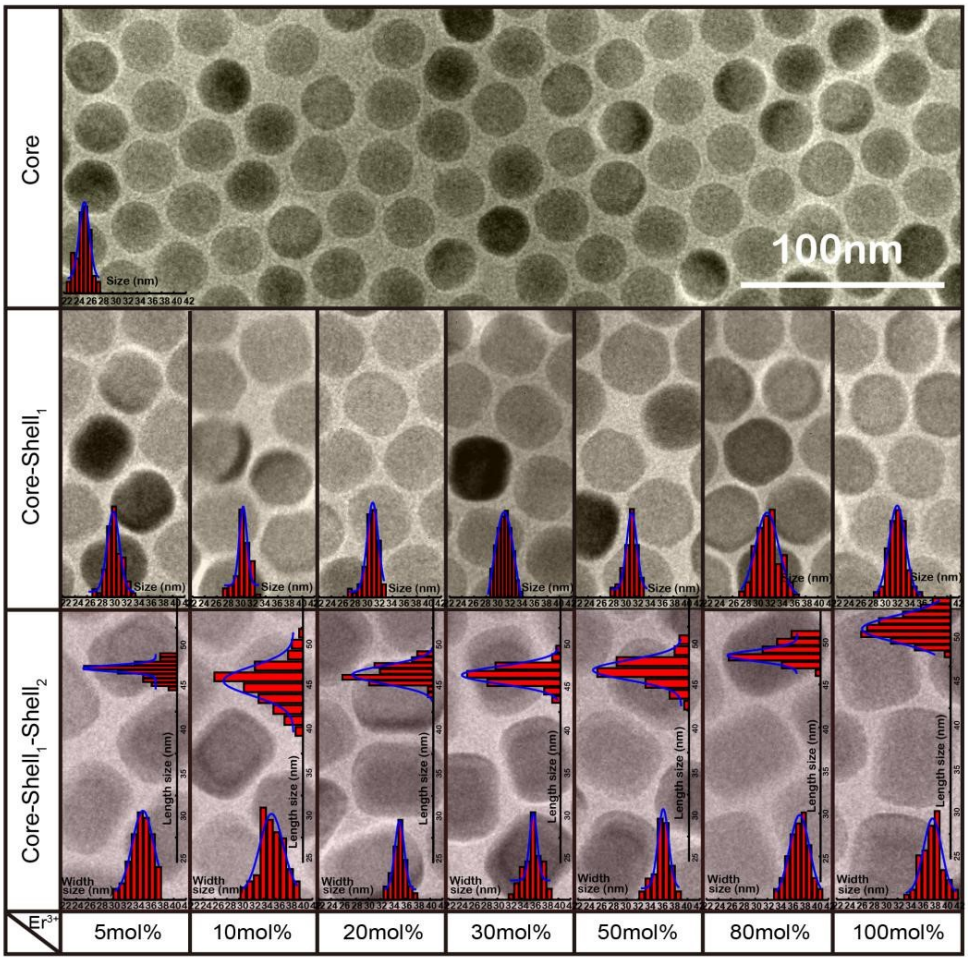

Fig. S17 TEM images and the corresponding size distributions (inset) of Yb,Ho core, Yb,Ho@xEr (x=5, 10, 20, 30, 50, 80, 100 mol%) core-shell, and Yb,Ho@xEr@Y core-shell-shell nanoparticles.

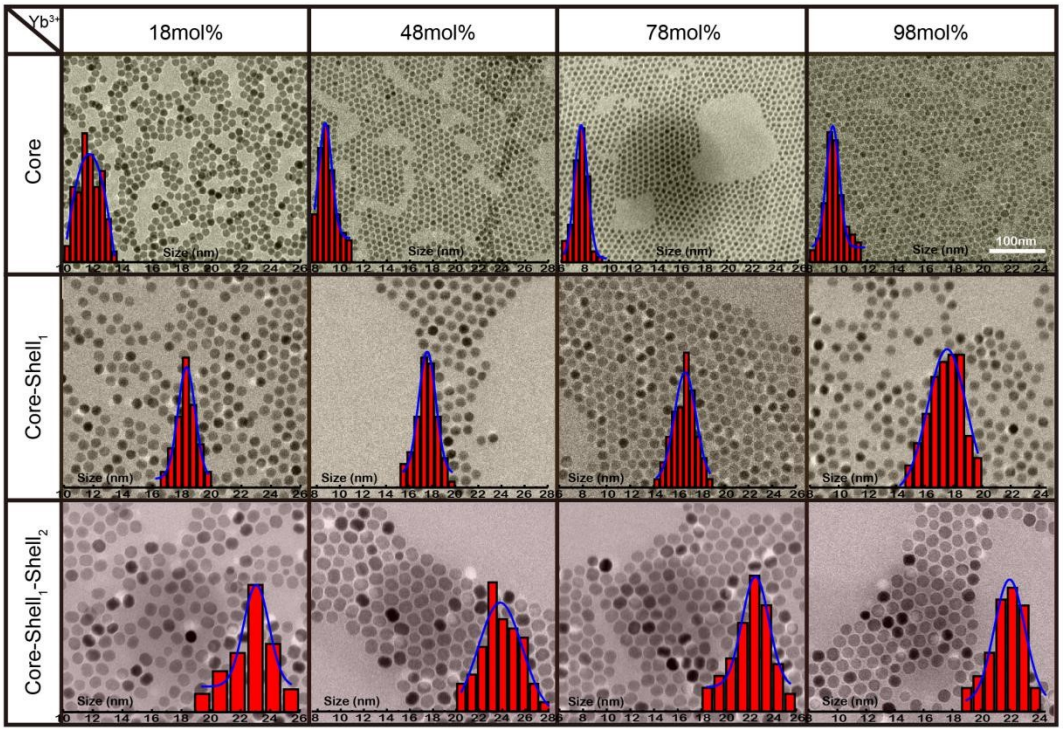

Fig. S18 TEM images and the corresponding size distributions (inset) of yYb,Ho (y=18, 48, 78, 98 mol%) core, yYb,Ho@Er core-shell, and yYb,Ho@Er@Y core-shell-shell nanoparticles.

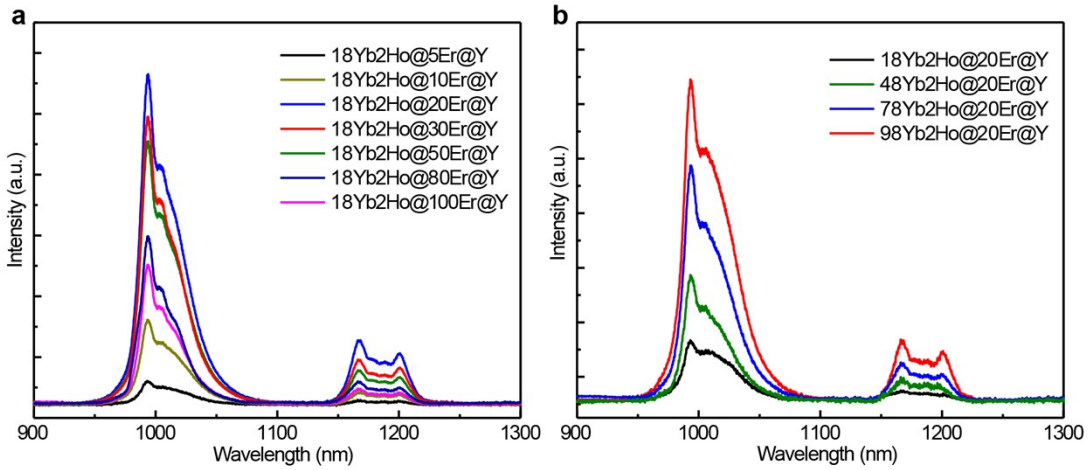

Fig. S19 Upconversion emission spectra of (a) Yb,Ho@xEr@Y (x=5, 10, 20, 30, 50, 80, 100 mol%) and (b) yYb,Ho@Er@Y (y=18, 48, 78, 98 mol%) nanoparticles. A detailed investigation shows that the NIR-II emission intensity of Ho^{3+} is closely dependent on the doping concentration of Yb^{3+} in the core and Er^{3+} in the interlayer. The upconversion emission intensity of Ho^{3+} at 1200 nm reaches the maximum with the continuously increasing of Yb^{3+} doping concentration at an optimal concentration of 20%Er^{3+} under 1550 nm pumping, indicating that higher Yb^{3+} concentration can harvest more excitation energy from Er^{3+} and finally sensitize Ho^{3+} ions.

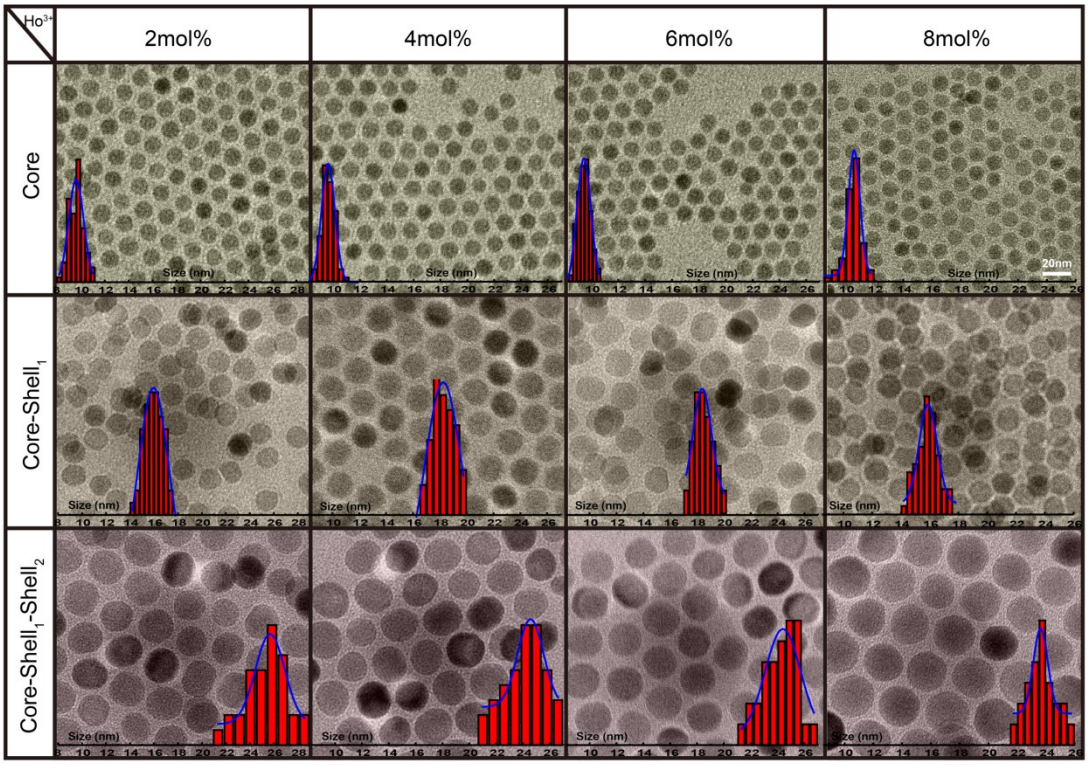

Fig. S20 TEM images and the corresponding size distributions (inset) of Yb,zHo (z=2, 4, 6, 8 mol%) core, Yb,zHo@Er core-shell, and Yb,zHo@Er@Y core-shell-shell nanocrystals.

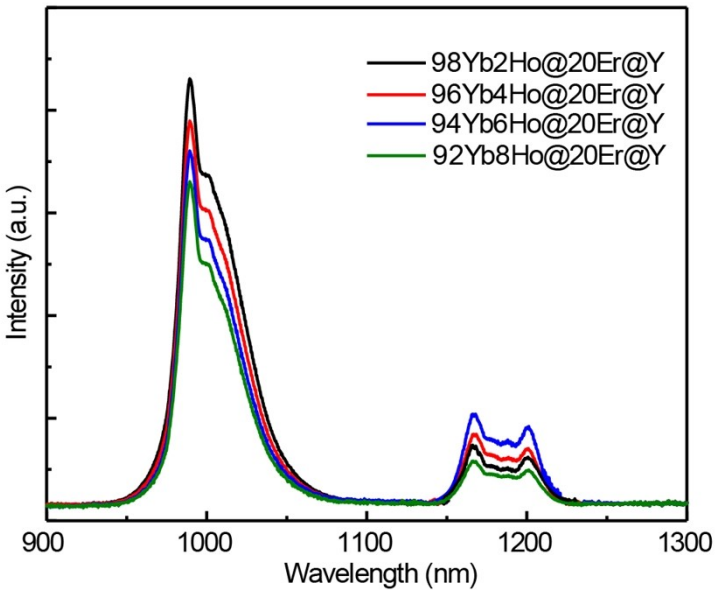

Fig. S21 Upconversion emission spectra of Yb,zHo@Er@Y (z=2, 4, 6, 8 mol%) upconversion nanocrystals under 1550 nm excitation.

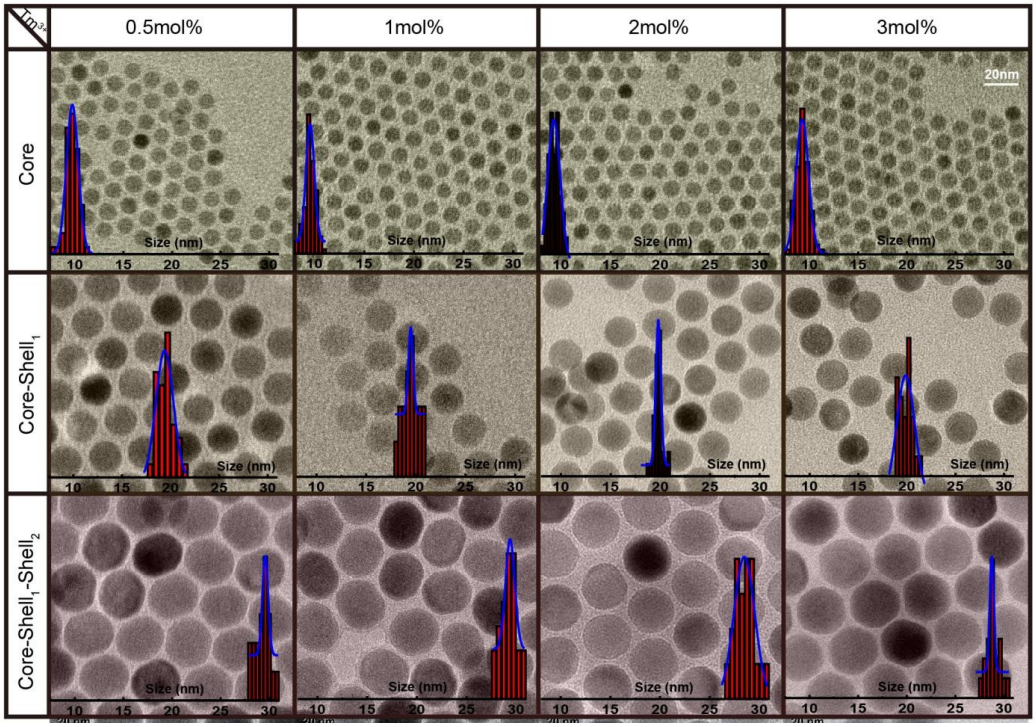

Fig. S22 TEM images and the corresponding size distributions (inset) of Yb,wTm (w=0.5, 1, 2, 3 mol%) core, Yb,wTm@Er core-shell, and Yb,wTm@Er@Y core-shell-shell nanoparticles.

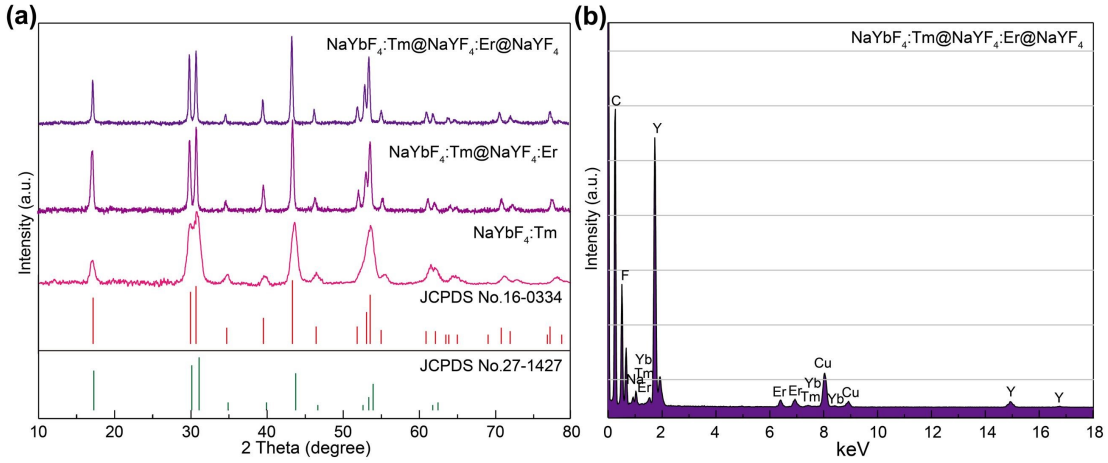

Fig. S23 (a) XRD patterns of Yb,Tm core, Yb,Tm@Er core-shell, and Yb,Tm@Er@Y core-shell-shell nanocrystals. (b) EDS spectrum of Yb,Tm@Er@Y upconversion nanocrystals. The XRD results prove the as-synthesized samples to be pure hexagonal phase. All the elements of Na^{+}, F^{-}, Y^{3+}, Tm^{3+}, Yb^{3+}, and Er^{3+} elements were detected by the EDS analysis. The strong signal of Cu and C elements are from original TEM copper grid and the presence of OA ligand on the particle surface, respectively.

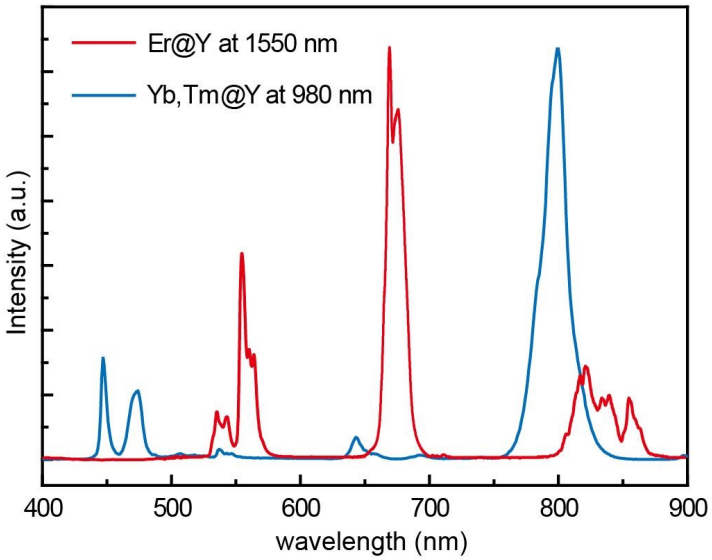

Fig. S24 Upconversion emission spectra of Er@Y excited by 1550 nm laser and Yb,Tm@Y excited by 980 nm laser. The wavelength positions of NIR emission of Er^{3+} and Tm^{3+} ions are different.

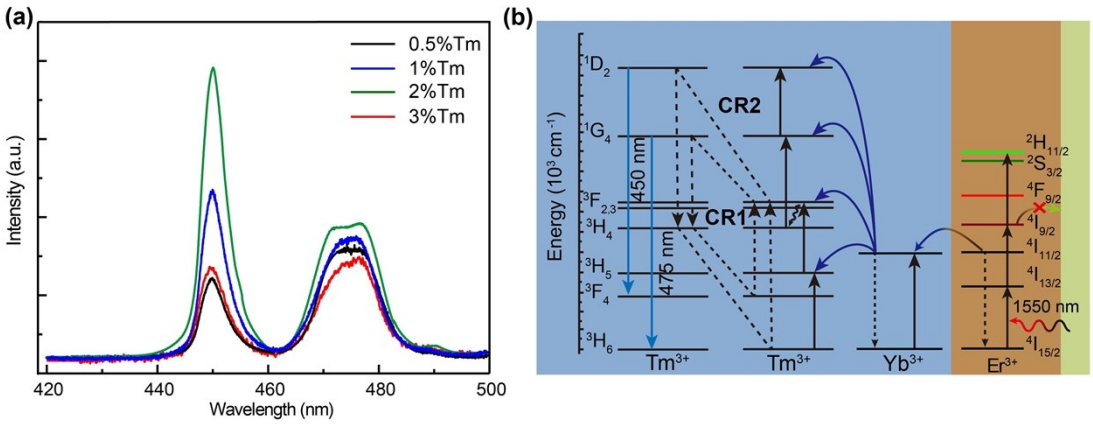

Fig. S25 (a) Blue emission spectra of Yb,wTm@Er@Y (w=0.5, 1, 2, 3 mol%) samples under 1550 nm excitation and (b) the schematic upconversion processes of the blue emissions. The 450 and 475 nm emissions arise from the $^1D_2 \rightarrow {}^3F_4$ and $^1G_4 \rightarrow {}^3H_6$ transitions of Tm^{3+}, respectively. The intensity ratio of I_{450}/I_{475} emission increases by increasing Tm^{3+} doping concentration from 0.5 to 2 mol%. This is due to the cross-relaxation process of $^1G_4 + {}^3F_4 \rightarrow {}^3H_4 + {}^3F_2$ (CR1), which becomes more efficient with Tm^{3+} doping concentration. This cross-relaxation process can lead to the population reduction of the $^1G_4$ state [9], thereby the I_{450}/I_{475} increasing with Tm^{3+} concentration. When further increase the Tm^{3+} concentration up to 3%, the cross-relaxation processes of $^1G_4 + {}^3F_4 \rightarrow {}^3H_4 + {}^3F_2$ and $^1D_2 + {}^3H_6 \rightarrow {}^3H_4 + {}^3F_2$ (CR2) quench both the 450 and 475 nm emissions due to concentration quenching effect [10]. Especially, the CR2 process has much influence on the population of the $^1D_2$ energy level at high Tm^{3+} ions doping concentration (3%), which dramatically quenches the 450 nm emission. Thus, the intensity ratio of I_{450}/I_{475} decreases at high Tm^{3+} doping concentration of 3%.

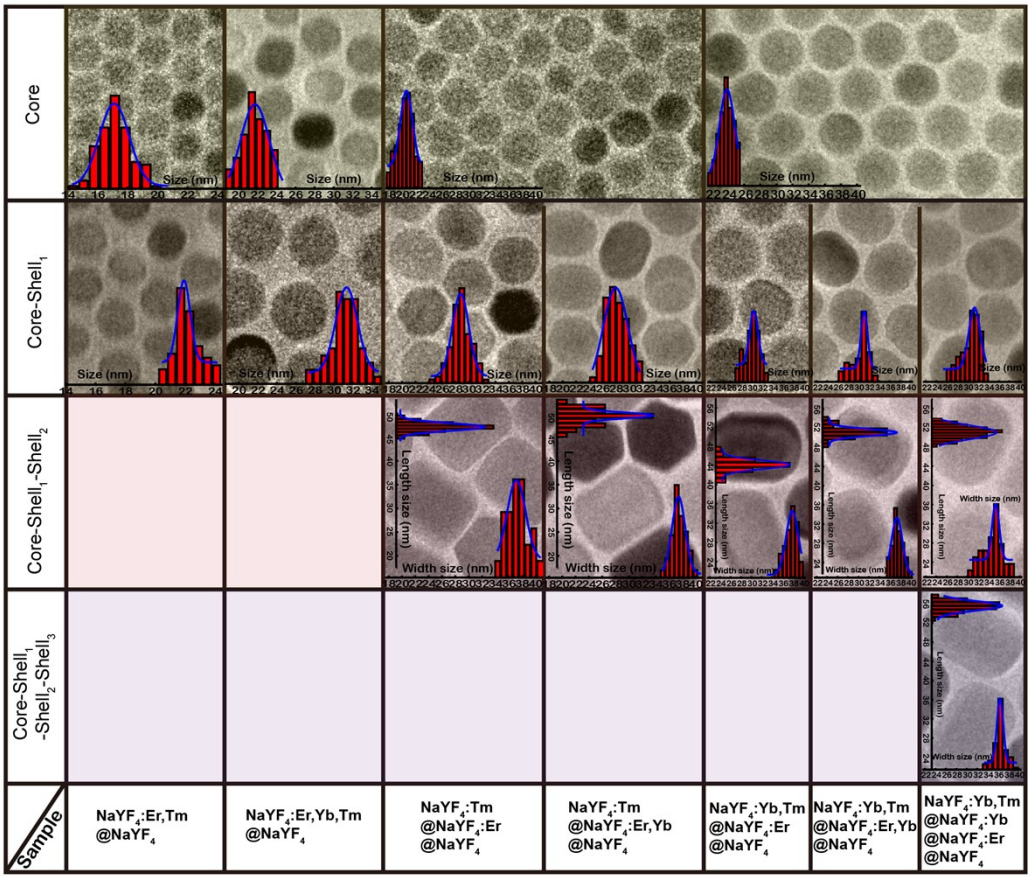

Fig. S26 TEM images and the corresponding size distributions (inset) of Er,Tm@Y, Er,Yb,Tm@Y, Tm@Er@Y, Tm@Er,Yb@Y, Yb,Tm@Er,Yb@$NaYF_4$, Yb,Tm@Er@Y, and Yb,Tm@Yb@Er@Y nanoparticles.

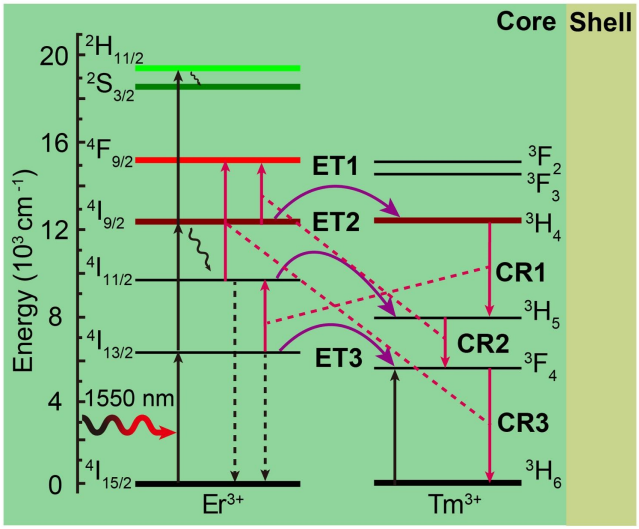

Fig. S27 Schematic upconversion processes in Er,Tm@Y nanoparticles. The ET1, ET2, CR1, and CR2 processes between Tm^{3+} and Er^{3+} could seriously quench the emission of Tm^{3+} and simultaneously enhance the population of the red-emitting state of Er^{3+} ion. Thus, we observed that red emission component of Er,Tm@Y and Er,Yb,Tm@Y upconversion nanoparticles are both enhanced compared with that of Er@Y.

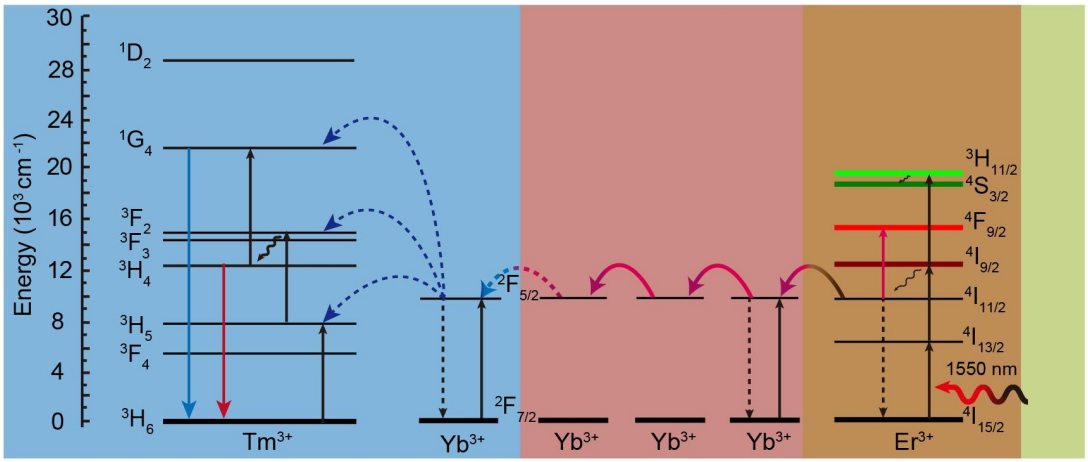

Fig. S28 Schematic upconversion processes in Yb,Tm@Yb@Er@Y nanoparticles.

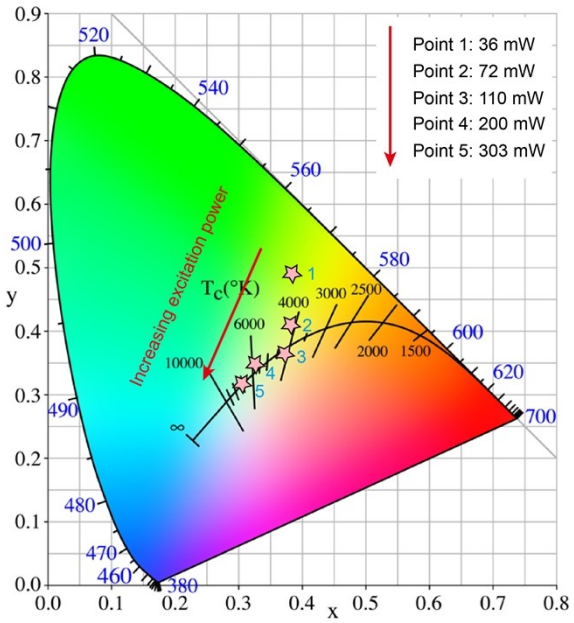

Fig. S29 The CIE chromaticity coordinates diagram of the Yb,Tm@Er@Y sample under 1550 nm excitation with the pumping power increasing from 36 to 303 mW.

Supplementary References

[1] L. Yan, B. Zhou, N. Song, X. L. Liu, J. S. Huang, T. Wang, L. L. Tao, Q. Y. Zhang, *Nanoscale,* 2018, **10**, 17949–17957.

[2] R. K. Shi, X. C. Ling, X. N. Li, L. Zhang, M. Lu, X. J. Xie, L. Huang, W. Huang, *Nanoscale*, 2017, **9**, 13739.

[3] F. Wang, Y. Han, C. S. Lim, Y. Lu, J. Wang, J. Xu, H. Y. Chen, C. Zhang, M. H. Hong, X. G. Liu, *Nature*, 2010, **463**, 1061–1065.

[4]J. C. de Mello, H. F. Wittmann, R. H. Friend, *Adv Mater.*, 1997, **9,** 230–232.

[5] C. Homann, L. Krukewitt, F. Frenzel, B. Grauel, C. Würth, U. Resch–Genger, M. Haase, *Angew. Chem. Int. Edit.*, 2018, **57**, 8765–8769.

[6] C. T. Xu, P. Svenmarker, H. Liu, X. Wu, M. E. Messing, L. R. Wallenberg, S. Andersson-Engels, *ACS nano*, 2012, **6**, 4788–4795.

[7] H. Liu, C. T. Xu, G. Dumlupinar, O. B. Jensen, P. E. Andersen, S. Andersson-Engels, *Nanoscale*, 2013, **5**, 10034–10040.

[8] R. Martín-Rodríguez, S. Fischer, A. Ivaturi, B. Froehlich, K. W. Krämer, J. C. Goldschmidt, B. S. Richards, A. Meijerink, *Chem. Mater.*, 2013, **25**, 1912.

[9] W. Wei, Y. Zhang, R. Chen, J. Goggi, N. Ren, L. Huang, K. K. Bhakoo, H. D. Sun, T. T. Y. Tan, *Chem. Mater.*, 2014, **26**, 5183–5186.

[10] G. Wang, W. Qin, L. Wang, G. Wei, P. Zhu, R. Kim, *Opt. Express*, 2008, **16**, 11907–11914.